

Volcano Monitoring Using Short Wavelength Infrared Data from Satellites

D. A. ROTHERY

Department of Earth Sciences, The Open University, Milton Keynes, England

P. W. FRANCIS

Lunar and Planetary Institute, Houston, Texas

C. A. WOOD¹

NASA Lyndon B. Johnson Space Center, Houston, Texas

Data from remote sensing satellites operating in the short-wavelength infrared can be used to measure temperatures of about 150°C and above. The gain settings of the Landsat Thematic Mapper (TM) sensors are such that to record pixel-integrated temperatures from 150°C to over 1000°C requires the use of several spectral bands. If the radiant source occupies less than a whole pixel, as is the case for fumaroles or a crusted lava surface with incandescent cracks, then the pixel-integrated temperature is less than the actual surface temperature of the hot areas and appears to be different at each wavelength. By determining pixel-integrated temperature in two spectral bands we can estimate both the temperature and size of hot areas which occupy less than a complete pixel. In some cases our observations provide the only available data on the state of activity of a particular volcano; in others they support and refine field observations. Our Landsat TM data reveal otherwise unobserved precursor and subsequent activity related to the September 1986 eruption of Lascar volcano (Chile) and supplement other data on the March 1986 eruption of Augustine volcano (Alaska). They also indicate the continued presence of lava lakes at Erta 'Ale (Ethiopia) in the absence of any ground-based observations and document minor eruptive activity at Mount Erebus (Antarctica). Landsat Multispectral Scanner data have been used to measure the variation in temperature along a lava flow on Sierra Negra (Galapagos Islands) which occurred in 1979.

INTRODUCTION

Volcanoes are among the few geological landforms which undergo changes at scales and rates sufficient to warrant frequent surveillance. Monitoring of volcanoes is important to document the course of their activity in order to model and thus to understand more fully their behavior. Monitoring is therefore an essential step toward the ultimate goal of predicting eruptions and their related hazards.

Apart from straightforward physical risk to personnel, the principal factor involved in the selection of techniques to use for volcano monitoring is cost effectiveness. Volcanoes with a known history of hazardous activity can be well instrumented and closely studied, but experience shows that the most serious eruptions take place on volcanoes with little or no record of historic activity (e.g., El Chichon, 1982; Nevado de Ruiz, 1985). There are probably several hundreds of volcanoes in the world which are as little known as El Chichon but which present comparable risks. Many of these volcanoes are remote and poorly accessible, which makes it difficult and expensive to mount a conventional field-based surveillance program. Even in easily accessible areas (such as Mount Etna) the altitude and physical extent of a typical volcano can cause logistical problems. The personal risks involved in observing active volcanoes on the ground or from low-altitude aircraft are well known. Remote sensing by satellite provides a hitherto little used technique for volcano monitoring, which we believe will be much more widely useful in the future.

Copyright 1988 by the American Geophysical Union

Paper number 7B1081.
0148-0227/88/007B-1081\$05.00

Meteorological satellites (e.g., GOES) provide low-resolution multispectral images which can be useful for tracking the development and dispersal of eruption clouds [Robock and Matson, 1983; Malingreau and Kaswanda, 1986; Sparks et al., 1986; SEAN, 1986a; Sawada, 1986]. Meteorological satellites have the great advantage that they provide frequent coverage of any individual area. We note that plans are being developed to use data from weather satellites to provide warnings to aircraft of volcanic ash clouds in their path [National Oceanic and Atmospheric Administration, 1987]. However, thermal infrared data at the low resolution provided by weather satellites (1-8 km) have proved rather inconclusive for observing magmatic events and their thermal precursors [Wiesnet and D'Aguanno, 1982; Bonneville et al., 1985; Bonneville and Kerr, 1987]. In this study we discuss short-wavelength infrared data from the present generation of high-resolution remote sensing satellites, which operate at pixel sizes less than 100 m across. Although the cost of purchasing the digital data is high (\$1650 for a quarter-scene magnetic tape of Landsat Thematic Mapper data and \$660 for a Landsat Multispectral Scanner scene), the quality of the information on surface conditions which can be extracted is greatly superior to that from meteorological satellites, although the relatively infrequent coverage is at present an important limitation. Future generations of satellites should offer more frequent coverage.

SHORT-WAVELENGTH INFRARED DATA

Measuring Pixel-Integrated Temperatures

The short-wavelength infrared region of the spectrum (0.7-3.0 μm), which is also known as the near infrared or reflected infrared, is not commonly regarded as suitable for thermal

LANDSAT TM TEMPERATURE SENSITIVITIES
(EMISSIVITY = 0.8)

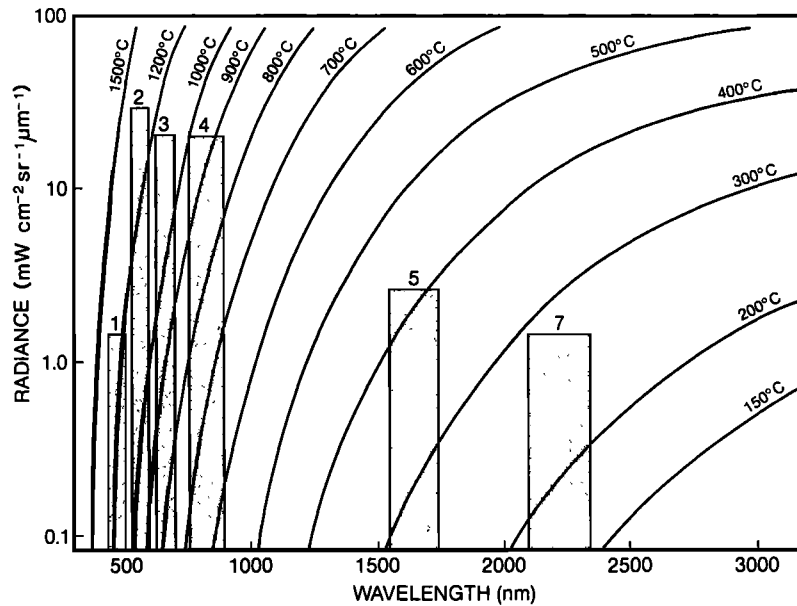


Fig. 1. Wavelength dependence of thermal radiance, according to Planck's formula, for surfaces with a uniform emissivity of 0.8, plotted for a range of temperatures. The lower limit of sensitivity of sensors on satellites is around $0.1 \text{ mW cm}^{-2} \mu\text{m}^{-1} \text{sr}^{-1}$. The boxes indicate the band passes and operational range of radiance for the visible and short-wavelength infrared Landsat Thematic Mapper (TM) sensors. TM data are quantized in 8-bits per channel, which means that there are 256 possible radiance (and hence temperature) values in each spectral band. The diagram is drawn on the assumption that all the at-satellite radiance is of thermal origin. If, as is usually the case in the visible and short-wavelength infrared, the thermal radiance is combined with reflected radiance, then the temperature at which the sensors become saturated is decreased. From Francis and Rothery (1987), with the labeling of the radiance units corrected.

monitoring. This is because at normally prevailing temperatures, surfaces radiate vanishingly small quantities of radiation in this region. Remote sensing satellites carry sensors operating in this part of the spectrum in order to take advantage of distinctive absorption features in the reflectance spectra of rocks and vegetation, such as the prominent hydroxyl absorption at $2.2 \mu\text{m}$. However, as dictated by Planck's formula, as temperature increases, so does the amount of energy radiated at all wavelengths, and especially at short wavelengths, and thus emitted thermal radiation can be detected by sensors designed for quite different purposes.

A sensor onboard a satellite is sensitive to upwelling radiation recorded as DN (digital number). The DN recorded in each spectral band by the Thematic Mapper (TM) and Multispectral Scanner (MSS) carried by the Landsat spacecraft can be converted into spectral radiance, measured in $\text{W m}^{-2} \mu\text{m}^{-1} \text{sr}^{-1}$, using the calibration data of Markham and Barker [1986]. If we can recognize that part of the spectral radiance R_λ which was radiated thermally from the surface, then we can use Planck's formula to relate this radiance to the kinetic temperature of the surface thus:

$$R_\lambda = \frac{\epsilon c_1 \lambda^{-5}}{\pi [\exp(c_2/\lambda T) - 1]} \quad (1)$$

where

$c_1 = 3.742 \times 10^{-16} \text{ W m}^2 = 2\pi h c^2$ (h is Planck's constant, c is speed of light);

$c_2 = 0.0144 \text{ m K} = hc/k$ (k is Boltzmann's constant);

λ wavelength, m;

ϵ emissivity of the radiating surface

T temperature, K;

Equation (1) can be rearranged to give T thus

$$T = \frac{c_2}{\lambda \ln([\epsilon c_1 \lambda^{-5} / \pi R_\lambda] + 1)} \quad (2)$$

Figure 1 shows the wavelength dependence of thermal radiance when it is of sufficient magnitude to be detected by satellite sensors in the visible and short-wavelength infrared region, plotted at various temperatures. It is evident that the short-wavelength infrared can be used to measure temperatures above about 150°C . The Landsat TM which has sensors at $2.08\text{--}2.35 \mu\text{m}$ (band 7) and $1.55\text{--}1.75 \mu\text{m}$ (band 5) is well suited for measuring temperatures, integrated over a pixel, in the range approximately $160^\circ\text{--}420^\circ\text{C}$. There is a gap in the TM pixel-integrated temperature coverage from around $420^\circ\text{--}700^\circ\text{C}$, between the saturation level of band 5 and the lower sensitivity limit of band 4 ($0.76\text{--}0.90 \mu\text{m}$). The shorter-wavelength TM sensors are capable of measuring pixel-integrated temperatures continuously from 700°C to over 1200°C . If the radiant material is concentrated in areas which cover less than a whole pixel, then the actual surface temperatures which are measurable increase within each band.

Thus, with its comparatively small nominal pixel size of 30 m by 30 m , the TM should in principle easily be capable of detecting and monitoring phenomena with temperatures typical of magmatic and fumarolic activity. In practice, it is uncommon

to find pixels radiating noticeably in the visible, and most of our studies are confined to the short-wavelength infrared. While image data in these wavelengths are of considerable value in a qualitative way for the detection and interpretation of volcanic thermal phenomena, several difficulties are involved in the use of short wavelength infrared and visible radiation for quantitative temperature measurements. Unlike the so-called thermal infrared ($>3.0 \mu\text{m}$) region of the spectrum, where there is negligible reflected solar radiation and therefore measured radiance is virtually all thermal in origin, thermal radiance at shorter wavelengths is combined (in daytime data) with solar radiance which has been reflected by the surface and scattered by the atmosphere. Any thermally radiant pixels which lie within shadow are prominent on such an image. Good examples of these are found when the thermal anomaly is located in a deep crater, fortunately a common volcanic situation. Since the pixels contain a negligible amount of radiance reflected by the surface, the amount of atmospheric backscattering can be estimated to a good approximation by equating it with the radiance sensed in nonthermally radiant pixels which are also in shadow. Thermally radiant pixels which are in sunlight (for example, a lava flow on an open surface) are also conspicuous by their anomalously high radiances at longer wavelengths but are more difficult to deal with. For these, the sum of reflected solar radiance and atmospheric backscattered radiance can be crudely estimated by comparison with the radiance sensed in sunlit but nonthermally radiant pixels which occupy similar rock types with similar slope aspects. In both the shadowed and sunlit cases the amount of thermal radiance is found by subtracting the estimated nonthermal radiance from the total detected radiance. Likely errors in pixel-integrated temperature for the sunlit case amount to around ± 10 K, except at the bottom of the temperature range for each band where the uncertainties become more significant.

There is a further source of error arising from the simplifying assumption that all the near-vertically upwelling thermal radiance reaches the sensor. In fact, some is absorbed and scattered by the atmosphere. This is difficult to quantify, but it is unlikely to exceed 10–20% for near-nadir viewing [Chahine, 1983] and would, in the absence of other sources of error, lead to pixel-integrated temperatures being underestimated by 5–10 K. We note that atmospheric absorption is likely to be most significant at sea level in humid environments. Fortunately, the volcanoes that we have studied have been located for the most part in high or arid environments. Accumulations of volcanic steam or other fumes over the hot area, perhaps trapped in a deep crater, might cause additional absorption. We consider that these errors are unimportant in most cases, in view of the additional uncertainties discussed below.

In order to use radiance to derive kinetic, or true, temperature of the surface rather than simply its apparent, or brightness, temperature, the emissivity of the surface must be known. This parameter is rarely measured directly. However, as a corollary of Kirchoff's law, emissivity equals absorptance, which is simply one minus the reflectance. This enables us to use our own and other data [e.g., Goetz *et al.*, 1983] on the short-wavelength infrared spectral reflectances of volcanic rocks to show that they mostly have emissivities between 0.5 and 0.9 in this part of the spectrum. The only factor that we have identified that may significantly alter the emissivity of hot and very fresh volcanic rock is encrustation by fumarolic sublimate minerals, such as sulphur, but this is unlikely to reduce emissivity below about

0.5. An uncertainty in emissivity of ± 0.2 gives rise to errors in pixel-integrated temperature of only about ± 15 K.

Pixel-integrated temperatures can actually be considerable underestimates of the true surface temperature of a thermal anomaly for two reasons: first, because the DN recorded for a pixel expresses the radiated energy integrated over the whole area of the pixel, whereas the actual anomaly may be much smaller, and second, because the radiance even from an anomaly somewhat bigger in size than a pixel may be shared between several adjacent pixels but never be the sole contributor to any one of them, depending on where the edges of the pixels fall relative to the anomaly. We will consider first the true size of the area sampled by each pixel, and its geometric implications, and then deal with the consequences of radiance distribution on the sub-pixel scale.

Pixel Size and the TM Point Spread Function

Although the nominal size of a Landsat TM band 1–5 and band 7 pixel is a 30 m by 30 m square, the area of terrain over which the radiance is collected to produce each image pixel is actually somewhat larger because of the optical characteristics of the system. The degree of optical blurring is conventionally measured by defining an effective instantaneous field of view for the sensor, which is taken to be limited by where the point spread function of the sensor falls to half its maximum value. Based on a variety of in-flight measuring criteria, the effective instantaneous field of view of the TM band 1–5 and band 7 optics has been variously reported in the range 33–46 m, and there is some evidence that its dimensions are greater in the scan direction than in the along-track direction [Anuta *et al.*, 1984; Schowengerdt *et al.*, 1985; Markham, 1985]. It is a reasonable approximation to assume that the area sampled by a TM “30 m” pixel is actually about 40 m across, which should be borne in mind when considering the information about hot volcanic features imparted by the TM data. The centers of adjacent pixels are 30 m apart, so there is an overlap zone about 10 m wide from which adjacent pixels are both sensitive to radiance. For the “120 m” pixels used in band 6 (thermal infrared), the effective instantaneous field of view appears to be about 140 m across.

Volcanic thermal anomalies generally cover rather small areas. To be sure that at least one 40 m by 40 m blurred TM pixel falls entirely within a circular thermal anomaly, wherever it lay in relation to the pixel array, its diameter would have to be about 113 m. The largest known lava lake at Kilauea, Hawaii, was at maximum 500 m in diameter [Jaggard, 1917] and would have filled of the order of 200 TM pixels. This, however, was exceptional. Most lava lakes and flows are broad enough to fill only a few pixels, and many pixels must be “mixed,” containing components both from the radiant source and the nonradiant background. We now consider the temperature ranges and spatial extent of volcanic thermal phenomena, and their implications for remote sensing.

Volcanic Thermal Phenomena

Volcanic thermal phenomena are often intrinsically rather small, as we will describe shortly. Because of the relationship between radiance and temperature (equation (1)), temperature estimates made on the assumption that a whole pixel is radiant are wrong if the radiance emanates unevenly from within the pixel. Consider, for example, a pixel with a radiant DN of

30 in TM band 5 and an emissivity of 0.6. This will have a temperature of 328°C if the radiance derives equally from throughout the pixel. However, if only part of the pixel is hot enough to radiate, we can calculate by simple proportion the radiance which would be detected if the whole pixel were radiant and use Planck's formula (equation (2)) to determine the temperature of the radiant area. Thus the same pixel could have a radiant area at 441°C, occupying 0.1 of a pixel, 607°C occupying 0.01 of a pixel or 873°C, occupying 0.001 of a pixel, in order to produce the same DN. The latter area corresponds to 1.6 m² in a blurred TM pixel, which is not unrealistic for an area of hot rock surrounding a high-temperature fumarole. Richter *et al.*, [1986] used similar arguments in using TM data to estimate the size and temperature of the area heated by fire resulting from the Chernobyl nuclear accident.

Volcanic thermal phenomena fall into three broad categories: low-temperature fumaroles, high-temperature fumaroles and lava-related effects.

Low-temperature fumaroles are the most common. They are typically exhalations of moist steam and sulphurous gases from small vents and fissure in the summit regions of volcanoes. Fumaroles of this kind are characteristic of the waning or passive phases of volcanism and are a surface expression of circulating ground waters being heated by contact with the still hot rocks within the core of the volcano. Although very common, these features are hard to detect remotely, since they are both small (often emanating from fissures only a few centimeters across) and cool (about 100°C or less, depending on the altitude of the volcano). These effects are too cold to affect the short-wavelength infrared, and although TM band 6 is sensitive in this temperature range, its coarse pixel size means that any anomaly is diluted by a large proportion of background, offering little hope of detection in daytime imagery. Night time TM band 6 data offer better possibilities, but in an examination of one night time scene from north Chile containing one large (Ollague) and two smaller (San Pedro, Aucanquilcha) known low-temperature fumaroles, no unambiguous thermal anomaly was detected.

High-temperature fumaroles are less common. They may release a variety of gases, ranging from superheated steam of groundwater origin to CO₂, SO₂, HCl, H₂S, and others at temperatures from a few hundred to over 1000°C. They provide evidence for the subsurface presence of a body of hot magma. In some cases, such as on basaltic volcanoes, a new batch of magma may de-gas by means of powerful fumarolic activity at one vent, while the lava itself is emitted quietly through a second vent, often at a lower altitude on the volcano (e.g. Mount Etna). Although often of small dimensions, of the order of 1 m, hot fumaroles may be measurable in TM bands 7 and 5 if the passage of the hot gases is able to heat the exposed rock surfaces up to comparable temperatures. There are few data as yet on this, but it is well known that the passage of hot gases through a fumarole vent is often sufficient to make the walls of the vent incandescent at visible wavelengths, implying temperatures of at least around 500°C. An important task for future volcanic thermal remote sensing is to develop techniques for discriminating between hot fumaroles and lava bodies.

Lava bodies are the third, and most obvious, form of volcanic thermal anomaly. One obvious distinction between these and high-temperature fumaroles is that lavas are spatially more extensive. The thermal structure of lava anomalies may be complex because of the formation of chilled crust even on the

most liquid basaltic lavas, which is broken by incandescent cracks as is well displayed on the familiar night time movie sequences of Kilauea. Surfaces of lavas with more evolved compositions do not develop "liquid" features but are characterized by boulder-sized chilled clasts, in which case, radiant areas may be confined to the interstices between blocks. As a result, the pixel-integrated temperature of any lava must be expected to be considerably less than that of the molten rock.

Thus many volcanic phenomena are likely to produce most of their radiance from only a part of each pixel, either because the hot area is intrinsically small (e.g., at a fumarole) or, as in the case of molten lava lake or flow, much of the surface consists of chilled crust and most of the radiance comes from narrow cracks distributed throughout the pixel. Table 1 illustrates the pixel-integrated temperatures and DN which would be recorded by the TM for a variety of realistic volcanological situations.

Wavelength Effects in Temperature Estimates Due to Subpixel Radiant Areas

In practice, we do not find the same pixel-integrated temperature for any pixel in two spectral bands, as demonstrated by the values in Table 1. This is due to the wavelength-dependent relationship between radiance and temperature, so that pixels which contain subpixel size radiant areas appear hotter at shorter wavelengths. If we assume that the highly radiant proportion of the pixel is the same in each of two spectral bands, which requires that the lateral temperature gradient is very high at the edge of the hot area(s) within the pixel, then we can use this relationship to find the highly radiant proportion of a pixel for which the derived temperatures are the same in each band. To do this, we must assume a temperature for the cooler, background, part of the pixel. The simplest case is when this is too cold to radiate significantly. This dual-band method provides a means of estimating both the size and temperature of hot areas which occupy less than a complete pixel [Dozier, 1981; Matson and Dozier, 1981].

In this study we estimate the radiant proportion of the pixel and its temperature by a graphical method, illustrated in Figure 2. This shows that, at typical DN values, if the assumed radiant DN is wrong by 20% in one band only, then the temperature derived by the dual-band method will be wrong by about 200 K and the radiant area will be incorrect by a factor of 2. Fortunately, the uncertainties in assumed radiance, whether due to emissivity factors or atmospheric absorption, are likely to be of similar magnitude in both bands, leading to much smaller errors in the dual-band method. Thus, if assumed emissivity in both bands is wrong by 0.2 or if atmospheric absorption amounts to 20% of the upwelling radiance in both bands, then the errors will be about 20 K in derived temperature and 20–40% in radiant area.

Other Errors

Further errors arise within the data themselves. Large radiance differences between terrain falling in adjacent pixels in the same scan line introduce the possibility of hysteresis in the sensor system, which would lead to slight undervaluing of DN in the upscan direction and overvaluing of DN in the downscan direction, at hot thermal anomalies. A potentially more serious problem lies in the resampling of the original pixels which occurs during geometric correction of the data. TM data are

TABLE 1. Apparent (Pixel-Integrated) Temperatures and DN Which Would be Measured by the Landsat Thematic Mapper for a Variety of Volcanic Features

Radiant Feature	Surface Temp. of Hot Area, °C	Hot Proportion of Pixel	Surface Temp. of Cold Area, °C	Pixel-Integrated Temperature, °C				DN			
				TM3	TM4	TM5	TM7	TM3	TM4	TM5	TM7
Lava fountain	1150	0.33	0-100	1054	(1031)	(932)	(873)	69	(498)	(38781)	(81241)
Lava lake crust at 550°C cracks at 1100°C	1150	0.1	550	926	886	(749)	(696)	13	98	(10604)	(28725)
Lava lake crust at 550°C cracks at 1100°C	1100	0.001	550	-	-	(555)	(552)	1	3	(1436)	(8984)
Lava lake crust at 400°C no cracks	400	1	-	-	-	400	(400)	1	1	129	(1518)
Lava lake crust at 200 °C cracks at 1100°C	1100	0.001	200	-	-	385	290	1	2	97	236
Pahoehoe flow (no crust)	1050	1	-	1050	(1050)	(1050)	(1050)	66	(600)	(73860)	(173893)
Pahoehoe flow crust at 200 °C cracks at 1050 °C	1050	0.01	200	-	706	(506)	(411)	2	7	(742)	(1767)
Blocky lava crust at 100 °C cracks at 1000 °C	1050	0.005	100	-	-	(460)	363	1	4	(372)	(872)
Pyroclastic flow	200	1	-	-	-	-	200	1	1	3	28
Hot fumarole	800	0.001	0-100	-	-	307	228	1	1	19	57
Cooler fumarole	600	0.001	0-100	-	-	243	179	1	1	5	16

Numbers in brackets are DN above the 0-255 range of the present TM system and temperatures which would be recorded if the dynamic range of the sensors were to be extended sufficiently. Temperatures too low to be measured are indicated by dashes. The examples cover a representative range of conditions. Temperature distributions of lava fountains and flows are based on the work by *Pieri et al.* [1985], those for fumaroles are based on the work by *Le Guern and Bernard* [1982] and the those for the hotter lava lake are based on the work by *Le Guern et al.* [1979] and *Le Guern* [1987].

geometrically rectified to "P format" during routine preprocessing at Goddard Space Flight Center. This can lead to the smoothing off of small-area, large-magnitude anomalies, resulting in artificially low-temperature estimates. We have been unable to find a quantitative analysis of this effect in the literature. The undervaluing of DN caused by resampling can be overcome by using raw, "A format" data. The calibration data for converting DN to radiance in digital images with this format can be found in the leader files on the computer compatible magnetic tape [*Earth Observation Satellite Company (EOSAT)*, 1985].

Errors may also be introduced because the data are acquired across a finite spread of wavelengths rather than at a single wavelength. In this study we have normally used the midpoint in the band pass of each sensor as the effective wavelength in equation (2). In fact, the effective wavelength depends on both the filter transmission characteristics of each sensor and the

radiant temperature of the surface. Errors in wavelength give rise to uncertainties of less than 10 K for pixel-integrated temperature and no more than 30 K in temperatures from the dual-band method.

The early Landsat 4 TM bands 5 and 7 were spatially misregistered by up to about 0.2 of a pixel, or about 6 m [*Anuta et al.*, 1984; *Wrigley et al.*, 1984]. This means that temperatures derived by the dual-band method will be in error by an amount which depends on the extent of the radiant area and where it sits in relation to the effective edges of the pixels in either band. The errors are potentially largest for very small, very hot radiant areas (for example, a 1-m-diameter 1000°C anomaly) but are negligible for dispersed radiant sources. Fortunately, the optical blurring of the pixels acts on a similar scale to the misregistration, so even a spatially small anomaly must always affect both bands in at least one pixel, allowing the temperature to be accurately estimated. However, depending on how the

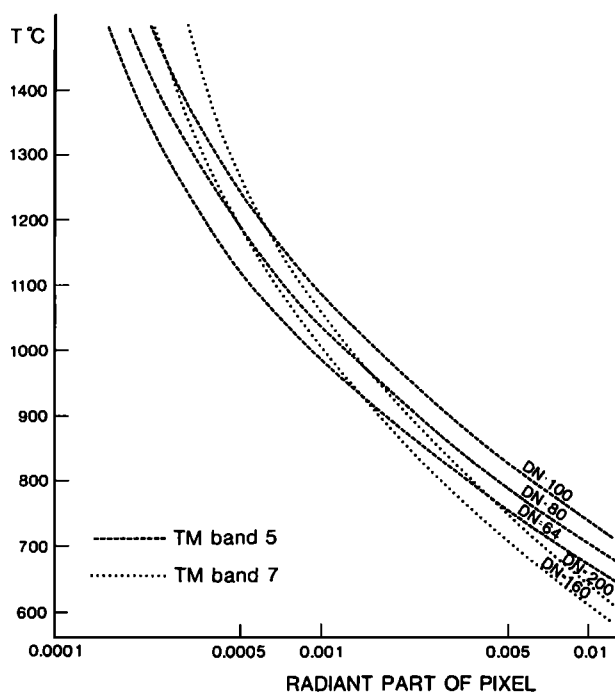


Fig. 2. Surface temperature of a radiant area occupying part of an otherwise nonradiant pixel and the size of that area expressed as a proportion of a pixel, calculated from selected radiant DN in Landsat TM bands 5 and 7. The assumed emissivity is 0.6. The solution for temperature and area when DN is measured in two bands is given by the crossover between the appropriate curves for the DN in each band. For example, if the radiant DN in band 5 is estimated to be 100 and that in band 7 to be 200, then the derived surface temperature is 1200°C emanating from about 0.0006 of a pixel. However, if the band 7 radiant DN has been miscalculated, for reasons discussed in the text, and should really be 160, then the corresponding surface temperature and area are 1450°C and 0.0003 of a pixel.

slightly misregistered pixels fall on the ground relative to the anomaly, it would be possible for the anomaly to be within the effective instantaneous field of view of an adjacent pixel in one band but not in the other band which would lead to a spurious dual-band temperature for that pixel. However, it should be possible to recognize and disregard this phenomenon on the images. It should be noted that a particularly hot anomaly could produce enough radiance to affect a pixel even when situated several meters beyond the edge of what is normally regarded as the effective instantaneous field of view; for example, the TM point spread function does not fall to 5% of its maximum value until about 30 m from the center of the pixel [Markham, 1985], whereas the edge of the effective instantaneous field of view, as usually defined is, only about 20 m from the center of the pixel. Errors would be greater for the dual-band method of temperature derivation using bands 4 and 5 together, due to the larger misregistration between bands 5 and 7 and the shorter-wavelength bands 1–4, which was reported to be as high as 0.6 of a 30-m pixel for early Landsat 4 TM data [Anuta *et al.*, 1984; Wrigley *et al.*, 1984].

In order to show how short-wavelength infrared data can be used in practice, we discuss below examples from several active volcanoes. "A format" TM data were available in only one case. We have usually assumed an emissivity of 0.6 in TM bands 5 and 7 and 0.8 in band 4, based on our unpublished reflectance data for volcanic rocks.

IMAGE DATA COVERING ACTIVE VOLCANOES

Lascaz Volcano, Northern Chile

We have previously reported our discovery of a thermal anomaly with a temperature of several hundred degrees centigrade within a summit crater of Lascaz (Figure 3), which was a precursor to a powerful explosive eruption on September 16, 1986 [Francis and Rothery, 1987; Rothery and Francis, 1987; SEAN, 1987]. Lascaz was the only volcano out of several hundreds examined in the central Andes to exhibit any significant thermal activity. A radiant area several pixels across is present in Landsat TM bands 5 and 7 on images acquired on March 16 and July 21, 1985 (pre-eruption), and scattered radiant pixels occur in October 27 and November 12, 1986, images (post-eruption). No pixels showed detectable radiance in band 4. Originally, we thought that the discrepancies we found between the temperatures measured in bands 5 and 7 were probably due to preferential absorption in band 7 caused by fumes. Since then we have found similar discrepancies on each active volcano that we have studied, and it now seems clear that this is likely to be mostly due to the effect of subpixel radiance discussed above.

The pre-eruption images of Lascaz show a radiant area about 100–150 m across at the center of a summit crater (Plates 1a and 1b). (Plate 1 is shown here in black and white. The color version can be found in the separate color section in this issue). Our original interpretation of this as a lava lake is supported by observations made during an aircraft overflight in January 1987. No magmatic activity whatever was visible at that time, but terraces on the sides of the crater confirmed that a lava lake had existed at some previous period. It is possible that these could have been inherited from an earlier lava lake and not be related to the 1985 lava lake. The pixel-integrated minimum temperature of 370°–380°C, which we previously reported for the pre-eruption anomaly, can be refined by combining data from bands 7 and 5 in the dual-band method described above. The July 1985 image is more useful since most of the radiant area lies in shadow. The dual-band method applied to the DN of the most radiant four pixels in the center of the anomaly suggests temperatures of 850°–1000°C occurring in hot areas occupying about 0.002–0.004 of each pixel, which may represent a small lava lake. Even at the maximum temperature and maximum radiant area suggested, this is consistent with the fact that there is no detectable radiance within any pixel in band 4. The central area is surrounded by a zone about two pixels wide with dual-band temperatures below 700°C, which almost certainly represent fumarolic activity. In the March 1985 image the anomaly is strongly sunlit, and the central, hottest, part is saturated in band 7 so that the dual-band temperature estimates cannot be made.

The pre-eruption temperature estimates of even the hottest part of the Lascaz anomaly are low in comparison with known lava lakes: for example, at Erta 'Ale in Ethiopia. *Le Guern et al.* [1979] report a variable amount of glowing lava covering an average of about 0.07 of the lava lake, at 1100°C, and a 2-cm-thick crust at 577°C covering the rest. This would have saturated TM bands 5 and 7. However, lava lakes are very variable, and a thicker crust with a lower surface temperature can develop if convection becomes slack enough [Tazieff, 1975], so it is possible that the Lascaz phenomenon was a less dynamic lava lake and had a thick, cooler crust. The only alternative possibility that we can envisage is a concentration of high-temperature fumaroles in the central region of the crater.

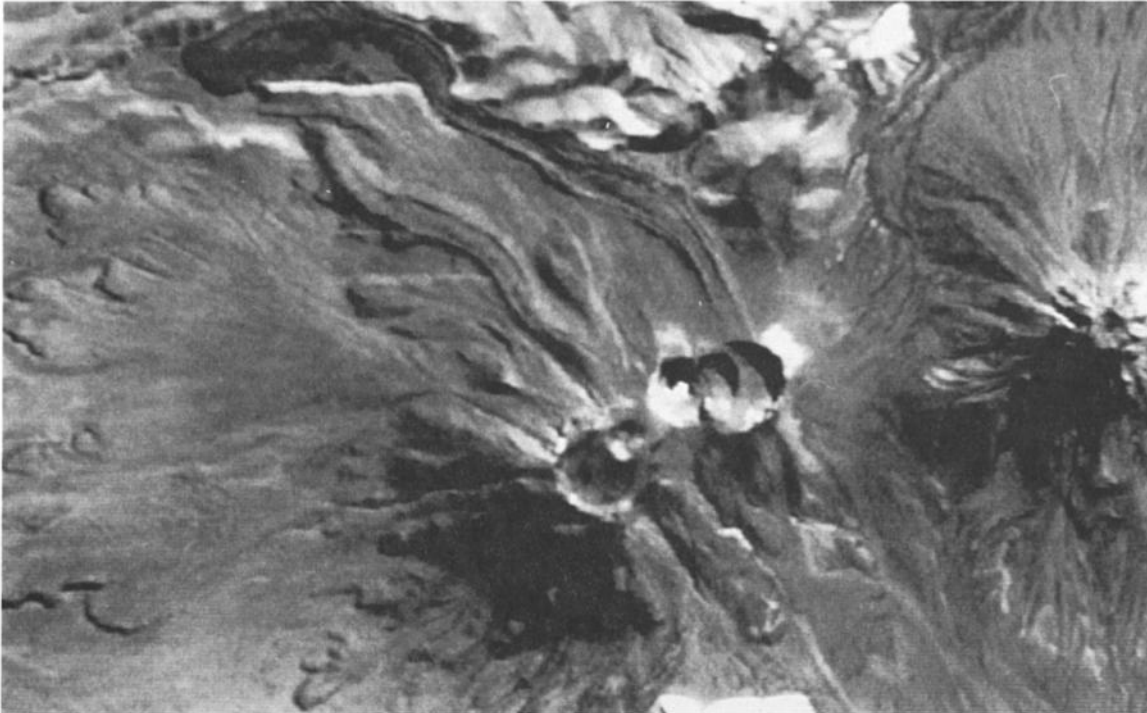


Fig. 3. Landsat TM band 7 image of the Lascar area, northern Chile, acquired July 21, 1985. Closeups of the summit area are shown in Plates 1a-1c.

After the September 1986 eruption the thermal area on the images is less well defined and consists of several isolated pixels (Plate 1c). Temperatures derived from the band 7 and band 5 dual-band method using A format data acquired on November 12, 1986, suggest temperatures of 680°–850°C deriving from 0.001 to 0.004 of a pixel. These temperatures together with the dispersed nature of the hot areas are suggestive of hot fumarolic activity rather than surface magmatism. Fumarolic activity was noted during the January 1987 overflight, and one fumarole vent appeared to correspond with the location of a hot area noted on the November 1986 image. A P format image acquired 16 days prior to the A format image shows a similar distribution of radiant pixels, but the derived temperature for the hottest ones is around 1200°C, occupying 0.001 of a pixel. This temperature is unrealistically high for a fumarole and may be due to undervaluing of the DN in band 7 due to resampling of the small-area anomaly, but it does suggest that temperature decreased between the dates of our two post-eruption images.

We conclude that the 1985 data provide evidence of either a magmatic (lava lake) or high-temperature fumarolic precursor to the September 1986 eruption. Lascar is not monitored on the ground, and this information would have been of value in notifying local geologists of the likelihood of forthcoming eruption had the phenomenon been discovered in time. The post-eruption data show that surface magmatism had ceased, but the high temperatures 2 months after the event suggest that Lascar remained more active than any other volcano in the central Andes, and the possibility of further eruptions can not be discounted. Further monitoring is clearly merited. Ideally, ground or aircraft-based observations would be made simultaneously with a satellite overflight, in order to determine the full extent to which fumarolic activity alone is capable of generating thermal anomalies detectable by the TM.

While we are unable to determine unequivocally whether the

pre-eruption thermal anomaly was due to the presence of a lava lake or fumaroles, it is important to emphasize that even if it were due to fumarolic activity, this must have been of high-temperature magmatic origin. We have carefully examined TM images of all the active volcanoes in the central Andes. Many of these have persistent fumarolic steam plumes. One (Guallatiri, north Chile) has a steam plume large enough to be visible for 100 km on the ground and for both it and its shadow to be visible on TM images. None of these volcanoes, however, shows any thermal anomaly in the short-wavelength infrared, and temperatures around the fumarole must be close to that of the steam, 80–90°C.

Augustine Volcano, Alaska

Augustine volcano, which forms an island in the Cook Inlet of Alaska, erupted about midnight on March 26–27, 1986, after a period of closely monitored precursor activity. Fortunately, Landsat 5 passed over on the morning of March 27, and the sky was clear. The resulting image has been widely distributed [e.g. *EOSAT*, 1986]. It provides a “snapshot” view of one episode of the eruption, which is a useful complement to ground-based observations made at the same time. An explosive event had clearly taken place shortly before the satellite came overhead, and a well-developed, dense ash cloud had risen to a height of several kilometers and had not yet begun to disperse. The image shows a thermal anomaly radiant in TM bands 5 and 7 occupying an area about 25 pixels (750 m) across at the summit. This is the source of the eruption column and may represent upcoming ejecta rather than any solid surface. Bands 7 and 5 were saturated across an area 12 pixels in width, but there is no detectable radiance in band 4; the pixel-integrated temperature thus exceeds 420°C but is less than 700°C.

The image also provides some interesting observations of

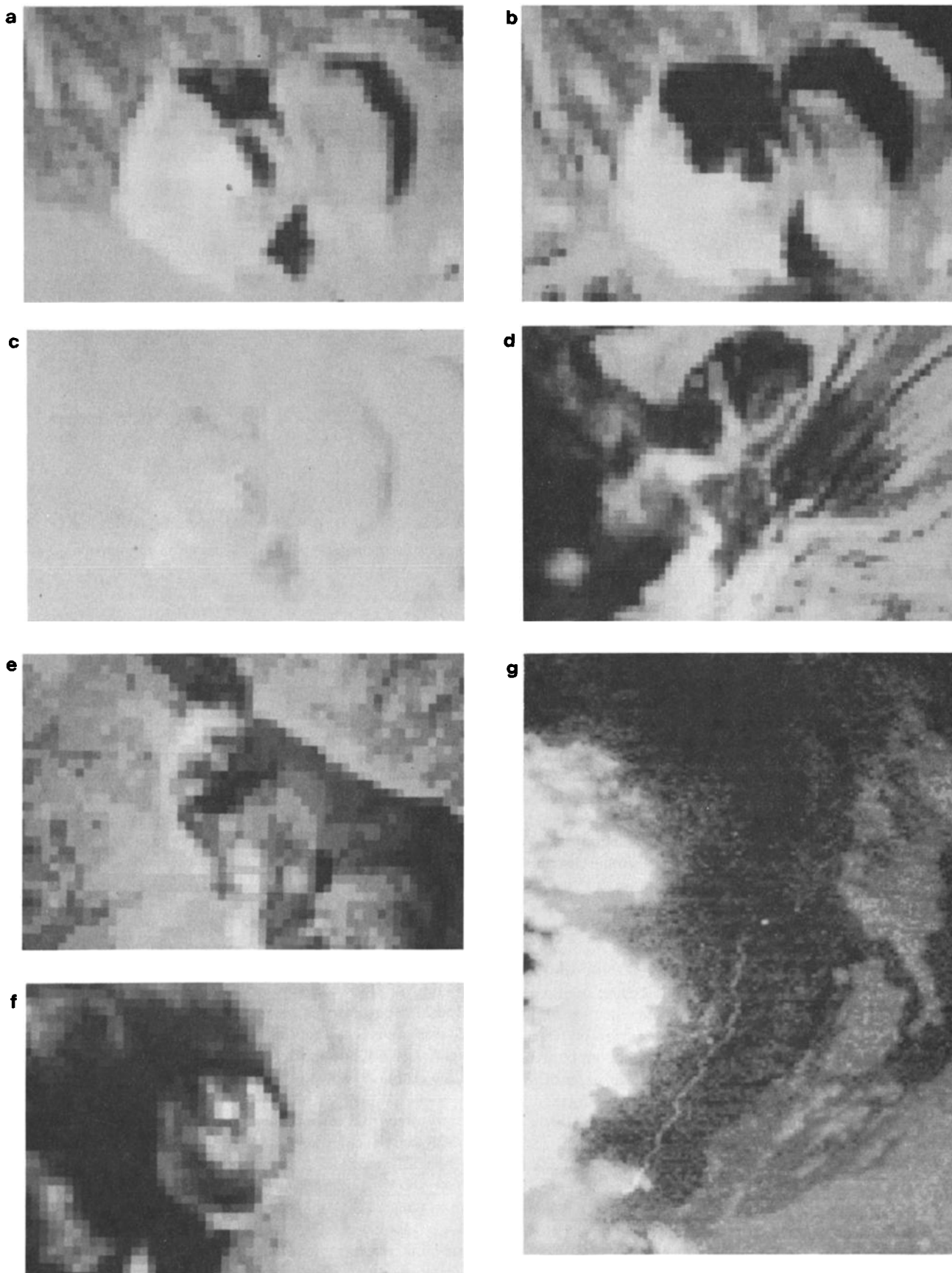


Plate 1. Landsat TM band 7, 5, 4 images (Plates 1a-1f) and Landsat MSS band 7, 6, 5 image (Plate 1g). (The color version and a complete description of this figure can be found in the separate color section in this issue.)

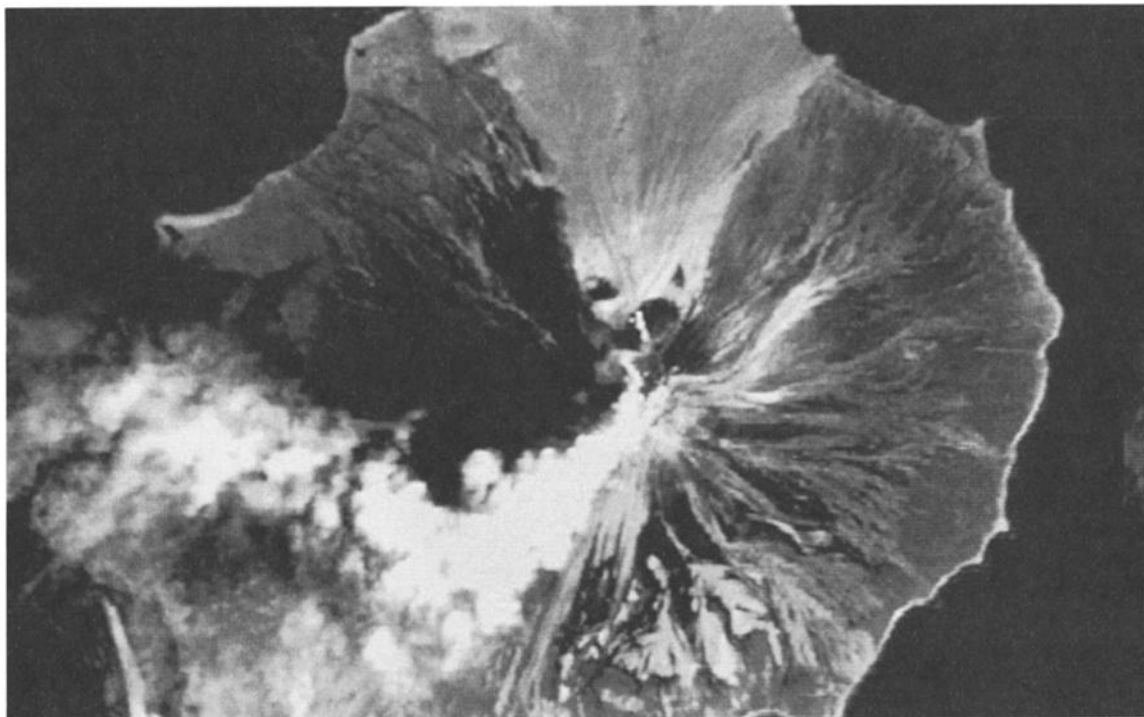


Fig. 4. Landsat TM band 7 image of Augustine volcano, acquired April 28, 1986. A close-up of the summit area is shown in Plate 1d.

pyroclastic flows and lahars. Some of the pyroclastic flows may have been emplaced less than an hour before the image was acquired, but because of their poor conductivity, their surfaces are too chilled to radiate in band 7 ($<160^{\circ}\text{C}$), although they are hot enough to saturate band 6 ($>70^{\circ}\text{C}$), where they are sufficiently wide to occupy whole 120 m by 120 m band 6 pixels. It is also significant that the pyroclastic flows are warmer at their margins than in the center; we attribute this to the concentration of larger pumice clasts in the marginal levees of the pyroclastic flows (cf. Mount St. Helens, 1980).

Augustine volcano continued to erupt for several months. A second TM image was acquired on April 28, 1986. This shows two radiant areas, both near the summit of the volcano (Plate 1d and Figure 4). The more northerly one is part of a blocky lava flow, the source of which is actually south of the radiant part of the flow. Field observations (T. P. Miller, personal communication 1986) showed that the radiant portion of the flow coincided with a steeper part of the slope, where fresh surfaces were continually being exposed as blocks broke away. Several pixels in this area are saturated in band 7 (indicating a pixel-integrated temperature of $>280^{\circ}\text{C}$) and one is also saturated in band 5 (indicating a pixel-integrated temperature of $>420^{\circ}\text{C}$), but none is radiant in band 4. For those pixels which are not saturated, the dual-band method suggests temperatures of $1050^{\circ}\text{--}1200^{\circ}\text{C}$ deriving from about 0.001 of a pixel.

The southerly radiant area on this image coincides with an active fissure trending toward the NNW. However, whereas visual observations made from a light aircraft and impeded by poor visibility suggested only a single fissure (T. P. Miller, personal communication 1986), the image clearly shows two en echelon features. As in the previous area, several pixels are saturated in band 7, and a few are saturated in band 5. For

unsaturated pixels the derived temperatures are $800^{\circ}\text{--}1300^{\circ}\text{C}$, occupying 0.003–0.0005 of a pixel.

The temperatures that we have derived for Augustine volcano are consistent with the very limited data available for field determinations of the temperatures of andesitic lavas [Cas and Wright, 1987]. Cigoline *et al.* [1984] report surface temperatures of $980^{\circ}\text{--}1020^{\circ}\text{C}$ measured by pyrometer and thermocouple at an andesitic vent on Arenal volcano, Costa Rica. We note that most available volcanic thermal data relate to basaltic eruptions; for example, Pieri *et al.* [1985] report maximum temperatures of about 1150°C in a lava fountain of Mauna Loa, based on helicopter-mounted thermal infrared radiometry, and Le Guern [1987] quotes a temperature of 1260°C for lava fountains at Niragongo. Meaningful temperatures are difficult to determine for andesitic and dacitic lavas because their surfaces are invariably blocky. The highest temperatures measurable in these circumstances will be those of escaping magmatic gases or of freshly erupting columns of ash and magmatic gases. Temperatures within eruption columns are difficult to determine from ground-based studies because of their opacity; it is possible that remote sensed data such as that from Augustine volcano may be able to contribute an additional source of data.

Augustine volcano has a history of collapse and tsunami generation [Kienle *et al.*, 1987] and thus presents a serious potential hazard to areas remarkably distant from the volcano itself. While the volcano itself is reasonably accessible to air observations, any additional information that satellites can provide which bears on the mechanical stability of the summit area at critical periods would clearly be of great value.

Erta 'Ale, Ethiopia

Erta 'Ale lies within the Afar region of Ethiopia and has been the site of lava lake activity since at least 1960 and probably

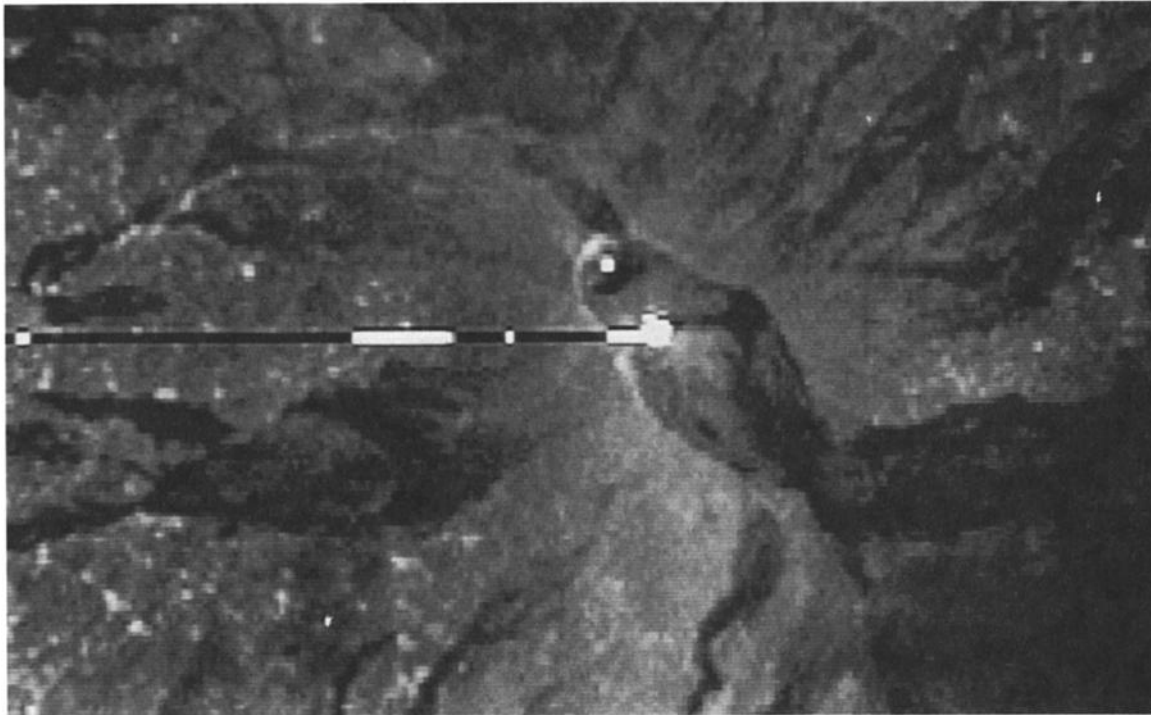


Fig. 5. Landsat TM band 7 image of Erta 'Ale, acquired January 5, 1986. A closeup of the summit area is shown in Plate 1e.

much before then [Mohr, 1962; Le Guern *et al.*, 1979]. Le Guern *et al.*, [1979] report that the summit region consists of an elliptical caldera 1600 m by 700 m in size, with its major axis oriented toward the NNW. During the years 1968–1974 this caldera contained two lava lakes, one in the north and the other near the center, both within steep-sided pits which sometimes overflowed, building perched lava lakes confined by spatter ramparts. The molten part of the northern lake varied between 70 m and 200 m in diameter, whereas the central one remained about 100 m across. They both rose in level during this period and actually overflowed in 1973 and 1974.

The latest field observations of which we are aware were made in February 1976, when the situation was much the same (G. Demisse, personal communication 1987). Our TM image (Plate 1e and Figure 5), which was acquired on 5 January 1986, therefore provides an important new datum. The image shows that the region of both lava lakes was still hot, but had changed significantly. The northern feature had become the smaller of the two, no more than 60 m across, whereas the central feature was now about 120–150 m in diameter. For the northern lava lake the dual-band method suggests temperatures in the range 800°–1100°C occupying 0.002–0.0004 of a pixel. In the central lava lake five pixels are saturated in band 7, one of which is also saturated in band 5, but there is no detectable radiance in band 4. The overloading of the band 7 sensor has had the effect of corrupting the band 7 data for over a hundred pixels down-scan from the anomaly. For those few pixels without saturation and which appear to have escaped the sensor overload effect, and which are suitable for the dual-band method, the derived temperatures are 570°–750°C occupying 0.003–0.008 of a pixel. These pixels are on the northern edge of this anomaly, and are presumably not typical of the whole, and the pixels which are saturated in band 7 almost certainly contain hotter and larger radiant sources.

We can put upper limits on the size and temperature of the hottest areas in the central anomaly, based on the observation that there is no thermal radiance detected in band 4. If the radiant areas were at 850°C, then they could make up about 0.05 of a pixel, before becoming detectable in band 4, whereas if they were at 1150°C, then they could occupy no more than about 0.004 of a pixel.

An alternative scenario could be the situation which prevailed at Erta 'Ale in 1971, when small areas of glowing lava at 1100°C were enclosed by a thin crust radiating at 570°C [Le Guern *et al.*, 1979]. In this case, both the glowing lava and the background would be hot enough to radiate. This situation would be detectable in band 4 if the hotter areas occupied more than about 0.006 of a pixel but would also saturate band 5 for mixtures in all proportions. As only one pixel on our image is saturated in band 5, although the central radiant area is several pixels across, we consider it unlikely that the situation described in 1971 prevailed when our image was acquired in 1986. We suggest that the central lava lake was probably present and larger in size, but in a quiescent state, and not subject to vigorous convective overturn. Its crust was thicker and had a maximum possible temperature of 400°C, otherwise all the pixels away from the edge of the anomaly would have been saturated in band 5. Glowing lava exposed in cracks in the crust was probably responsible for the saturation in bands 7 and 5, though the proportion of the area occupied by 1150°C glowing lava must have been less than 0.004.

To determine how representative the January 6, 1986, image is of the recent configuration of Erta 'Ale, we have examined a hard copy (photographic) band 7 image acquired on February 9, 1987. This shows the same large radiant region in the central crater and a trace of an anomaly at the site of the northern lava lake, indicating little change during the intervening 13 months. While our interpretations are clearly tentative, we note

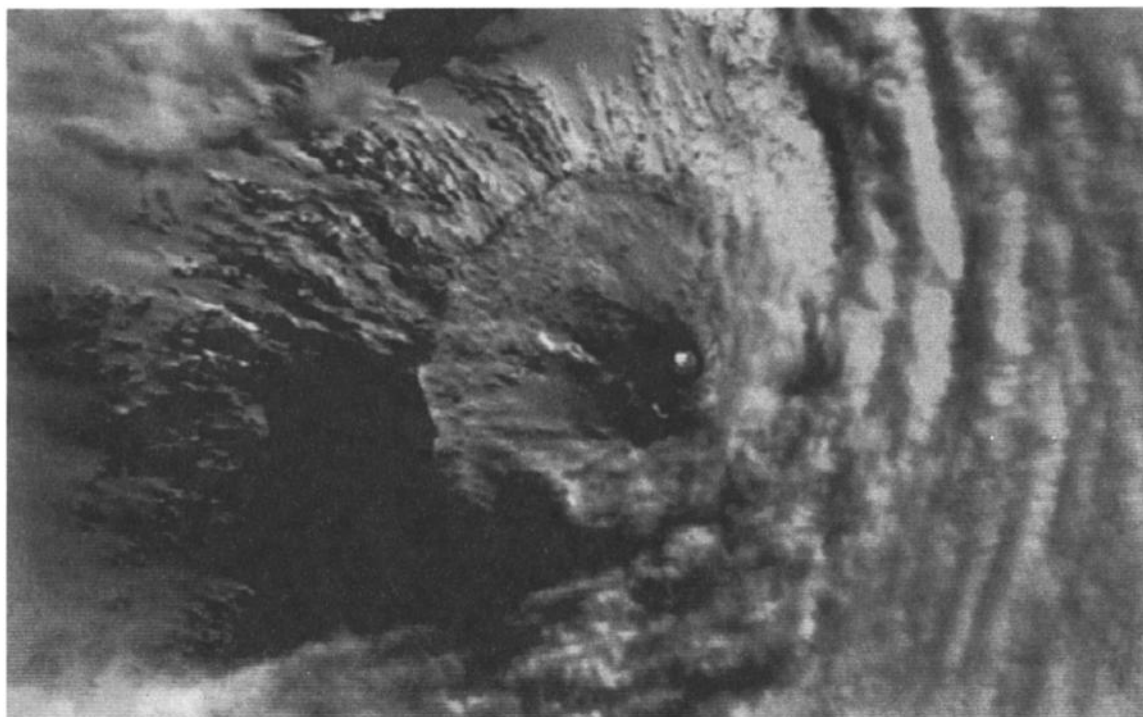


Fig. 6. Landsat TM image of Mount Erebus, made by combining bands 7 and 4 and acquired January 26, 1985. A close-up of the summit area is shown in Plate 1f.

that our observations on Erta 'Ale are the first on this major volcano for more than a decade.

Mount Erebus, Antarctica

The lava lake within the summit crater of Mount Erebus was first seen in 1972 [Giggenbach *et al.*, 1973]. It was present in all reported observations until October 20, 1984, by which date it had frozen and domed upward [SEAN, 1984] leaving only a small vent containing incandescent material near the center and scattered fumaroles on the frozen lake surface. Seismograms recorded about 10 or more explosions per day from September 1984 until February 1985. The first field observation of a new lava lake was in December 1985, when a 15-m-diameter lava lake occupied the pre-1984 site [SEAN, 1986b]. From November 1986 through early January 1987 the lava lake was 50 m wide and continuously active. Fumaroles are also reported to be consistently active around the summit crater (P. Kyle, personal communication, 1987).

We have examined a TM image of Mount Erebus acquired on January 26, 1985 (Plate 1f and Figure 6), which falls in a gap between the reported direct field observations. This image shows six pixels which are radiant in band 5, some of them saturated in band 7, surrounded by a circular radiant area in band 7 which is about 210 m in diameter. Where feasible, the dual-band method suggests temperatures of 900°–1130°C, occupying 0.001–0.002 of a pixel, which is compatible with optical pyrometer measurements of 1000°C made of the Mount Erebus lava lake in 1981 [Kyle *et al.*, 1982]. Bearing in mind the optical blurring of TM pixels, the size of the hotter, inner area affecting six pixels is likely to have been between about 30 and 50 m across, which is greater than that of the incandescent vent of the previous October. It is possible that the Mount Erebus lava lake was reestablished several months earlier than

can be proved from field observations, or alternatively, the image may record an enlarged incandescent vent.

The wide warm halo surrounding the central hottest area and which radiates only in band 7 has a surface temperature of about 240°C if the radiance comes evenly from the whole pixel and must contain hotter areas if the radiance emanates from only part of each pixel. Given that there is no detectable radiance in band 5 and assuming that the rest of the pixel is nonradiant, we can find the range of possible surface temperatures for the hot areas in each pixel which would produce a total radiance below the detection limit in band 5 but falling within the observed range for band 7. In fact, there are no solutions above about 400°C, and the hottest possible areas on a nonradiant background which tally with the data are areas at 400°C occupying about 0.05 of a pixel. This temperature distribution would be consistent with fumaroles only if they were widely and evenly dispersed throughout the halo, and we interpret this instead as representing a zone of recently erupted volcanic spatter. It is clear that the skin temperature of such, initially molten, spatter must cool rapidly, especially in the conditions of low ambient temperature and high winds prevailing at Mount Erebus, but we are not aware of any studies on the rate of cooling. However, in this instance we can interpret the halo of cooling spatter revealed on the TM image to be the product of an eruption associated with a small earthquake recorded by the International Mount Erebus Seismic Study (IMESS) seismic net on the volcano. During early January 1985 these events took place about 10–30 times a day, and there was one at 1951:36 UT (R. R. Dibble, personal communication 1987), just 5 min. before our image was acquired. Although there is no direct proof of an eruption, events of this sort at Mount Erebus are typically associated with eruption of small volumes of spatter, as documented by rim-based video recordings made from December 1986 to January 1987 by R. R. Dibble.

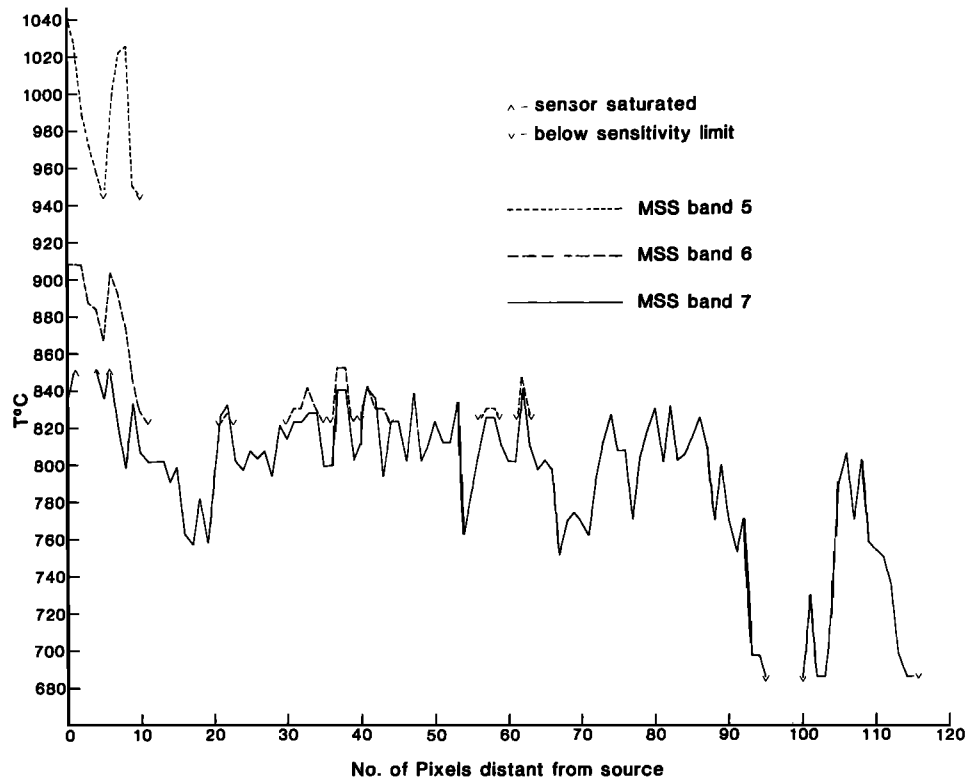


Fig. 7. Pixel-integrated temperatures measured from Landsat MSS data along the line of most radiant pixels along the Sierra Negra lava flow, November 19, 1979. MSS pixels are sampled on a rectangular grid of 58 m by 79 m.

If our interpretation is correct, then we are fortunate that the eruption occurred so shortly before the satellite overpass. Had it occurred, say, 10 min earlier, the surface temperature of the spatter is likely to have become too low to cause detectable radiance in TM band 7, and the image would merely have shown the hot pixels in the immediate vicinity of the vent.

Sierra Negra, Galapagos Islands

Landsat TM data have been available only since 1982, whereas the archive of Landsat MSS data extends back to 1972. The MSS lacks the longer-wavelength sensors carried by the TM and therefore cannot detect such low pixel-integrated temperatures, and each pixel contains radiance sampled from a comparatively large area, having an instantaneous field of view of about $79 \text{ m} \times 79 \text{ m}$ convolved with a blur circle of about 30 m diameter [Slater, 1979]. However, MSS data provide a cheaper way of monitoring sufficiently large events, and old MSS data can be used to obtain useful information about events which went unnoticed or were poorly observed at the time. As an example of this, we cite an eruption of Sierra Negra volcano (Isabela island, Galapagos archipelago), which began explosively on November 13, 1979. The plume was noted on images from a meteorological satellite, which prompted one of us (C.A.W.) to request immediate image acquisition by the Landsat MSS which revealed lava eruption in progress [SEAN, 1979]. As far as we are aware, no ground observations of any kind were made of the erupting lava, and so the only thermal information available is that which can be retrieved from the MSS data.

Our image was acquired by Landsat 3 on November 19, 1979, and shows a lava flow 1–3 pixels wide extending from near

the summit towards the sea 20 km away (Plate 1g). Near the source, the flow radiates in MSS bands 5, 6, and 7, and radiance in MSS band 7 can be traced for about 10 km before becoming too faint to be detectable. There is more dust and fumes in the air than on any of the TM images we have examined, and this is responsible for an indeterminate amount of scattering and absorption of the upwelling thermal radiance. This is exacerbated by the fact that we are using shorter wavelengths than with TM data. The dual-band method of temperature determination yields unrealistically high values. Markham and Barker [1987] describe several sources of radiometric inaccuracy which could account for this. However, estimates of the pixel-integrated temperature can be used to constrain the minimum average surface temperature of the flow. Figure 7 is a graph of pixel-integrated temperature plotted along the line of greatest radiance along the flow. In Table 2 we compare our results with those of Pieri *et al.* [1984] for a similar flow on Mauna Loa, and it can be seen that our results are consistent.

SUMMARY

We have demonstrated the ability of Landsat data to provide useful, and sometimes unique, information on magmatic and fumarolic events at poorly monitored active volcanoes and in one example (Lascar) to detect a precursor to an explosive event. By using radiant energy in the short-wavelength infrared we are able to measure temperatures which would saturate conventional thermal infrared devices. Where radiance is measurable in two spectral bands, the dual-band method enables us to estimate the temperature and size of the radiant portion of each pixel. When further ground truth studies are available,

TABLE 2. Comparison of Thermal Infrared Temperatures for a Basaltic Flow in Hawaii [Pieri *et al.*, 1985] with MSS Visible and Near-Infrared Temperatures for a Similar Flow in the Galapagos Islands

	Volcano			
	Mauna Loa, Hawaii	Sierra Negra, Galapagos		
Date	7 April 1984	November 19, 1979		
Source	Pieri <i>et al.</i> [1985]	this study		
Instrument	helicopter radiometer	Landsat MSS		
Range	30 m	920 km		
Wavelength(s), μm	10.6	0.8-1.1	0.7-0.8	0.6-0.7
Temperatures				
Fire fountain	700-1150°C			
Near source		>852°C	870-910°C	950-1030°C
Upper reaches				
Upper reaches	700-800°C*	800-840°C	810-850°C	-
8 km (crust)	500-700°C	700-800°C	-	-
10 km		685°C		
Active front	500-600°C†	<685°C	-	-

*No crust.

†At this point the interior temperature, which could be monitored within evolving fissures, was 900-1000°C.

this may allow us more definitely to distinguish between the presence of lava and fumaroles.

Coarse resolution (79 m pixel) Landsat MSS data in the very near infrared (wavelengths shorter than 1.1 μm) can be used to derive temperatures on sufficiently large areas with pixel-integrated temperatures in excess of about 640°C. Such conditions are likely to be met only on broad lava flows and especially active large lava lakes. The Landsat TM is more useful in that it has better resolution (30 m pixels) and sensors which operate further into the short-wavelength infrared. It is sensitive to pixel-integrated temperatures of about 160°C and above and is appropriate for observing both fumarolic and magmatic phenomena.

VOLCANOLOGICAL IMPLICATIONS

Quantitative and even qualitative volcano thermal monitoring by satellite is of great practical importance if major populations are threatened by volcanic activity, as at Augustine volcano. The high price of Landsat data (about \$14,000 for the digital data used in this study) could inhibit its use for routine monitoring, but the costs of using satellite data become more reasonable when compared with the expense involved in establishing and maintaining a program of field-based monitoring and are trivial compared to the economic damage done by a catastrophic eruption.

The implications of the ability to monitor volcanoes remotely

THERMAL RADIANCE AND LANDSAT TM TEMPERATURE SENSITIVITIES (EMISSIVITY = 0.8)

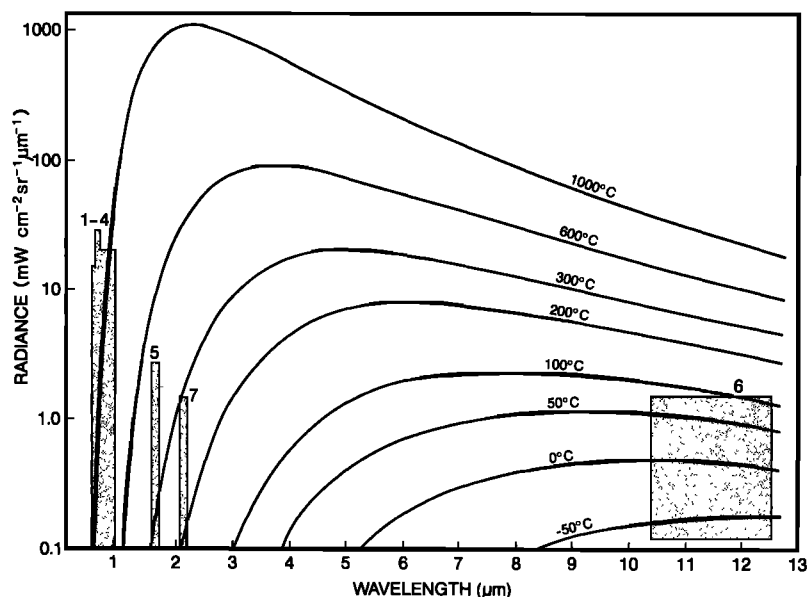


Fig. 8. Thermal radiance at various temperatures for surfaces with a uniform emissivity of 0.8 from the visible to the thermal infrared. An increase in emissivity of 0.2 would move the curves upward by 25% and a decrease in emissivity would move the curves downward by the same amount. Note the logarithmic radiance scale. The boxes indicate the operational range of the Landsat TM sensors. The band 7 sensor could cover temperatures from 200°C to over 1000°C only if its gain were reduced to operate over 3 orders of magnitude in radiance (0.1-1000 $\text{mW cm}^{-2} \text{sr}^{-1} \mu\text{m}^{-1}$). In order for the band 6 sensor to operate from 100°C to over 1000°C, its gain would have to operate over less than 2 orders of magnitude.

with existing technology are considerable; the implications offered by feasible future technologies are much greater, and offer exciting opportunities to advance our understanding of volcanic processes.

At the level of existing technology, the most obvious benefit of volcanological remote sensing is the simple ability to identify active volcanoes. This can be done by simple qualitative judgement, without requiring sophisticated data reduction. Cost factors aside, the most serious limitation to such studies at present is the 16-day orbital repeat of Landsat, since volcanic phenomena can and do change over much shorter time scales. The only high-resolution satellite system in operation other than Landsat is SPOT, which operates at a pixel size of 20 m for multispectral data. SPOT data are sold at commercial rates comparable with those for Landsat TM data. Unlike the Landsat TM, the SPOT imaging system is pointable, allowing more frequent repeat coverage. At present, SPOT carries sensors confined to wavelengths shorter than 0.9 μm , making it incapable of measuring pixel-integrated temperatures below about 700°C. However, with numerous nations developing and launching remote sensing satellites (United States, Japan, Canada, Russia, France, European Space Agency, etc.) the potential to obtain timely data for a given volcano becomes much greater. At present, delays of up to several months may intervene between the acquisition of data by a satellite and its delivery to an analyst, and these need to be overcome by streamlining the data handling at the ground station. Cloud cover presents a much more serious problem, as many volcanoes in humid regions are obscured by cloud for weeks consecutively.

Given these limitations, a second important benefit of volcanological remote sensing with existing technology is the ability to monitor change in a volcano already known to be active. This may range from detection of gross changes, such as the eruption of a new lava flow or formation of a new crater, which can be done using data in photographic format, to measurement of changes in temperature of existing thermal anomalies, requiring numerical analysis of digital data. The circumstances in which this ability is likely to be most useful are where it is important to obtain early warning of a possible eruption, for example, in the case of a major ice-covered volcano such as Ruiz, where even a small eruption may have devastating consequences. Most of our work has dealt with short-wavelength manifestations of hot phenomena, but we note that TM band 6 offers the opportunity to monitor changing temperatures of crater lakes such as those at Ruapehu (New Zealand) and Poas (Costa Rica), which have temperatures of the order of 50°C.

Where relatively stable volcanic thermal phenomena exist, such as long-lived lava lakes, existing technologies would also allow estimates of volcanic thermal budgets to be made, complimenting and extending field-based studies [e.g., *Helz and Thornber*, 1987]. At sites such as Erta 'Ale, where a lava lake has existed for decades, but no major lava flows have been erupted, it is clear that the volcano represents a site where heat, but not material, is constantly being transferred to the surface of the Earth. This is an aspect of volcanism that has been little studied.

FUTURE REMOTE SENSING SYSTEMS FOR VOLCANO MONITORING

SPOT 4 is due for deployment in the early 1990s and will carry an extra channel at 1.58–1.75 μm , roughly equivalent to TM band 5, but without an equivalent of TM band 7 which

precludes dual-band temperature measurements except for features sufficiently hot to affect the 0.9- μm region. Current plans for the sensor system to be carried by Landsat 7 [*Goward and Taranik*, 1986] suggest four new channels in the 8 to 14- μm region of the spectrum with 60-m pixels and one in the 3 to 5- μm region with 120-m pixels, but these are likely to saturate at brightness temperatures of 100°C or less. We consider below the wavebands and sensitivities required for sensors appropriate for volcano observations.

The steepness of the Planck radiance curves (Figure 1) within the usual sensitivity range of visible and short-wavelength infrared sensors means that sensors in several wavebands are required in order to cover completely the possible range of volcanic pixel-integrated temperature. To cover the whole of this range at with a single short-wavelength infrared channel would require drastic, and probably unfeasible, reduction in the gains of existing sensors. For example, a sensor operating in the same waveband as Landsat TM band 7 would require a gain decreased by 3 orders of magnitude in order to be sensitive across a radiance range of 0.1–1000 $\text{mW cm}^{-2} \text{sr}^{-1} \mu\text{m}^{-1}$, thus covering the range 200°–1000°C. If it were possible to construct such a sensor, then it could detect pixel-integrated temperature differences of about 4 K on 8-bit data by quantizing the radiance values in a logarithmic fashion.

The thermal infrared could also be used for measuring volcanic temperatures; a suitable sensor would be one in the 10 to 12- μm region, which would need to be sensitive from about 1 to 20 $\text{mW cm}^{-2} \text{sr}^{-1} \mu\text{m}^{-1}$ in order to measure pixel-integrated temperatures of 100°–1000°C (Figure 8). This is more or less the same gain as the present 120-m pixel Landsat 6 data and the 1-km pixel NOAA polar orbiter AVHRR data but operating over a different range with its lower end near the upper end of the ranges used at present. In principle, the higher radiances being detected by such a sensor should enable the size of the sensor elements, and hence the pixel dimensions, to be decreased below that used in current systems measuring nonvolcanic ambient surface and atmospheric temperatures. Between this region and the short-wavelength infrared there is only one other part of the spectrum in which the atmosphere transmits electromagnetic radiation, which is the 3 to 5- μm region in which the NOAA polar orbiters also have a sensor, AVHRR channel 3, at about 3.8 μm , which saturates at a pixel-integrated temperature of about 50°C. This region has considerable potential for use in volcano monitoring, and its use and particular sensitivity in fire detection are well known [*Muirhead and Cracknell*, 1985, 1986; *Matson et al.*, 1987].

Plausible future technologies are most likely to offer imaging spectrometers operating at about 10-nm spectral resolution (e.g., HIRIS), variable viewing geometries, and more frequent coverage of individual volcanoes. While it seems unlikely that future pixel sizes will be significantly better than those of the Landsat TM, the ability to measure thermal radiance at two or more wavelengths will make it possible to interpret structure at the subpixel level by use of dual-band techniques. It is possible that such sensors will be placed in geostationary orbit and thus offer the potential to monitor volcanoes on an essentially continuous basis. While this could represent a major advance over existing systems, cloud cover will continue to be a limitation. Night time coverage would reduce errors due to poor correction for reflected sunlight in the short-wavelength infrared, but make it hard to relate radiant features to their nonradiant surroundings. Processing of the large amounts of data inherent

in maintaining surveillance will present problems, but these can be minimized by selection of specific targets to be monitored. Apart from the general hazard warning aspects, continuous monitoring of volcanoes opens up a new range of volcanological studies, such as the tracking of the development of a new lava field and predicting the likely paths of newly erupted flows, and detailed studies of thermal budgets.

Acknowledgments. Thematic Mapper research is undertaken at the Lunar and Planetary Institute (LPI), Houston under NASA contract NAS 5 28759 and at The Open University, England. The LPI is operated by the Universities Space Research Association under contract NASW 4066. This paper is LPI contribution 647. Geologists and technicians at the MINSAL facility at Toconao, Chile, provided invaluable eyewitness accounts and photographs of the eruption of Lascar. Tom Miller of the U.S. Geological Survey Anchorage provided us with the background material on Augustine volcano. Getahun Demisse of the Ethiopian Institute of Geological Survey discussed the activity of Erta 'Ale with us. Vince Salomonson and John Barker of the Goddard Space Flight Center helped us understand the characteristics of TM data. Alexander Goetz and an anonymous reviewer provided helpful comments on the manuscript. Figures 3–6 and Plates 1a–1f are included by permission of EOSAT Corporation.

REFERENCES

- Anuta, P. E., L.A. Bartolucci, E.M. Dean, D.F. Lozano, E. Malaret, C.D. McGillem, J.A. Valdes and C.R. Valenzuela, LANDSAT-4 MSS and thematic mapper data quality and information content analysis, *IEEE Trans. Geosci. Remote Sens.*, *GE-22*, 222–235, 1984.
- Bonneville, A., and Y. Kerr, A thermal forerunner of the 28th March 1983 Mt. Etna eruption from satellite thermal infrared data, *J. Geodyn.*, *7*, 1–31, 1987.
- Bonneville, A., G. Vasseur, and Y. Kerr, Satellite thermal infrared observations of Mt. Etna after the 17th March 1981 eruption, *J. Volcanol. Geotherm. Res.*, *24*, 293–313, 1985.
- Cas, R. A. F., and J.V. Wright, *Volcanic Successions: Modern and Ancient*, p. 528, Allen and Unwin, London, 1987.
- Chahine, M. T., Interaction mechanisms within the atmosphere, in *Manual of Remote Sensing*, vol. 1, edited by R. N. Colwell, pp. 165–230, American Society of Photogrammetry, Falls Church, Virginia, 1983.
- Cigolini, C., A. Borgia, and L. Casertano, Intra-crater activity, aa-block lava, viscosity and flow dynamics: Arenal volcano, Costa Rica, *J. Volcanol. Geotherm. Res.*, *20*, 155–176, 1984.
- Dozier, J., A method for satellite identification of surface temperature fields of subpixel resolution. *Remote Sens. Environ.*, *11*, 221–229, 1981.
- Earth Observation Satellite Company, *User's Guide for Landsat Thematic Mapper Computer-Compatible Tapes*, Earth Observation Satellite Company, Lanham, Maryland, 1985.
- Earth Observation Satellite Company, Augustine volcano thematic mapper image, in *Landsat Data Users Notes*, vol. 1, pp. 1–2, Lanham, Maryland, 1986.
- Francis, P. W., and D.A. Rothery, Using the Landsat thematic mapper to detect and monitor active volcanoes: An example from Lascar volcano, northern Chile, *Geology*, *15*, 614–617, 1987.
- Giggenbach, W.F., P.R. Kyle, and G.L. Lynn, Present volcanic activity on Mt Erebus, Ross Island, Antarctica, *Geology*, *1*, 135–136, 1973.
- Goetz, A.F.H., B.N. Rock, and L. C. Rowan, Remote sensing for exploration: An overview, *Econ. Geol.*, *78*, 573–590, 1983.
- Goward, S.N., and J.V. Tarantik, Commercial applications and scientific research requirements for TIR observations of terrestrial surfaces, *Report of Joint EOSAT/NASA TIR Working Group*, NASA/EOSAT, Washington, D.C., Aug. 1986.
- Helz, R. T., and C.R. Thornber, Geothermometry of Kilauea Iki lava lake, Hawaii, *Bull. Volcanol.*, *49*, 651–668, 1987.
- Jaggard, T. A., Volcanological investigations at Kilauea, *Am. J. Sci.*, *44*, 161–220, 1917.
- Kienle, J., Z. Kowalik, and T.S. Murty, Tsunamis generated by eruptions from Mount St. Augustine volcano, Alaska, *Science*, *236*, 1442–1447, 1987.
- Kyle, P.R., R. Dibble, W. Giggenbach, and J. Keys, Volcanic activity associated with the anorthoclase phonolite lava lake, Mt Erebus, Antarctica, in *Antarctic Geoscience*, edited by C. Craddock, pp. 735–745, University of Wisconsin Press, Madison, 1982.
- Le Guern, F., Mechanism of energy transfer in the lava lake of Niragongo (Zaire), 1959–1977, *J. Volcanol. Geotherm. Res.*, *31*, 17–31, 1987.
- Le Guern, F., and A. Bernard, A new method for sampling and analyzing volcanic sublimates—Application to Merapi volcano, Java, *J. Volcanol. Geotherm. Res.*, *12*, 133–146, 1982.
- Le Guern, F., J. Carbonelle, H. Tazieff, Erta 'Ale lava lake: Heat and gas transfer to the atmosphere, *J. Volcanol. Geotherm. Res.*, *6*, 27–48, 1979.
- Malingreau, J. P., and Kaswanda, Monitoring volcanic eruptions in Indonesia using weather satellite data: The Colo eruption of July 28, 1983, *J. Volcanol. Geo. Res.*, *27*, 179–194, 1986.
- Markham, B. L., The Landsat Sensors' spatial responses, *IEEE Trans. Ge. Remote Sens.*, *GE-23*, 864–875, 1985.
- Markham, B. L., and J.L. Barker, Landsat MSS and TM post-calibration dynamic ranges, exoatmospheric reflectances and at-satellite temperatures, *EOSAT Tech. Notes 1*, pp. 3–8, Earth Obs. Satell. Co., Lanham, Maryland, 1986.
- Markham, B. L., and J.L. Barker, Radiometric properties of U.S. processed Landsat MSS data. *Remote Sens. Environ.*, *22*, 39–71, 1987.
- Matson, M., and J. Dozier, Identification of subresolution high temperature sources using a thermal IR sensor., *Photogramm. Eng. Remote Sens.*, *47*, 1311–1318, 1981.
- Matson, M., G. Stephens, and J. Robinson, Fire detection using data from NOAA-N satellites, *Int. J. Remote Sens.*, *8*, 961–970, 1987.
- Mohr, P. A., The Ethiopian rift system, *Bull. Geophys. Obs., Haile Sellassi Univ., Addis-Ababa, Ethiopia*, *5*, 33–62, 1962.
- Muirhead, K., and A.P. Cracknell, Identification of gas flares in the North Sea using satellite data, *Int. J. Remote Sens.*, *5*, 827–833, 1985.
- Muirhead, K., and A.P. Cracknell, Straw burning over Great Britain detected by AVHRR, *Int. J. Remote Sens.*, *6*, 199–206, 1986.
- National Oceanic and Atmospheric Administration, FAA consider volcano monitoring system, *Aviat. Week Space Technol.*, *127*, 30–31, 1987.
- Pieri, D., A.R. Gillespie, Kahle, A. B., and S.M. Baloga, Thermal infrared observations of lava flows during the 1984 Mauna Loa eruption. Reports of Planetary Geology and Geophysics Program: 1984, *NASA Tech. Memo.*, *87563*, 204–205, April 1985.
- Richter, R., F. Lehmann, R. Haydn, and P. Volk, Analysis of Landsat TM images of Chernobyl, *Int. J. Remote Sens.*, *7*, 1859–1867, 1986.
- Robock, A. and M. Matson, Circumglobal transport of the El Chichón volcanic dust cloud, *Science*, *221*, 195–197, 1983.
- Rothery, D. A., and P. W. Francis, Detection and monitoring of volcanic activity using short-wavelength infrared TM and MSS imagery, paper presented at the Annual Conference of the Remote Sensing Society, University of Nottingham, Sept. 7–11 1987.
- Sawada, Y., Detection capability of explosive eruption by GMS image and behaviours of dispersing eruption cloud, paper presented at International Volcanological Congress, Inter. Assoc. Volcanol. Chemistry Earth's Interior, Auckland-Hamilton-Rotorua, New Zealand, 1986.
- Schowengerdt, R. A., C. Archwamety, and R. C. Wrigley, Landsat thematic mapper image-derived MTF, *Photogramm. Eng. Remote Sens.*, *51*, 1395–1406, 1985.
- SEAN, Sierra Negra, *SEAN Bull.*, *4*, 3–6, 1979.
- SEAN, Mount Erebus, *SEAN Bull.*, *9*, 1984.
- SEAN, Augustine Volcano, *SEAN Bull.*, *11*, 2–8, 1986a.
- SEAN, Mount Erebus, *SEAN Bull.*, *11*, 16–18, 1986b.
- SEAN, Lascar Volcano, *SEAN Bull.*, *11*, 3–4, 1987.
- Slater, P. N., A re-examination of the Landsat MSS, *Photogramm. Eng. Remote Sens.*, *45*, 1479–1485, 1979.

- Sparks, R. S. J., J.G. Moore, and C.J. Rice, The initial giant umbrella cloud of the May 18th, 1980, explosive eruption of Mount St Helens, *J. Volcanol. Geotherm. Res.*, 28, 257-274, 1986.
- Tazieff, H., *Niragongo, the Forbidden Volcano*, Flammarion, Paris, 1975, (Published in English by Cassell, London 1979).
- Wiesnet, D. R., and J. D'Aguanno, Thermal imagery of Mt Erebus from the NOAA-6 satellite, *Antarct. J. U.S.*, 17, 32-34, 1982.
- Wrigley, R. C., D. H. Card, C. A. Hlavka, T. R. Hall, F. C. Mertz, C. Archwamety and R. A. Schowengerdt. Thematic Mapper image quality: registration, noise and resolution. *IEEE Transactions on Geoscience and Remote Sensing*, GE-22, 263-271, 1984.
-
- P. W. Francis, Lunar and Planetary Institute, 3303 NASA Road One, Houston, TX 77058
- D. A. Rothery, Department of Earth Sciences, The Open University, Milton Keynes, MK7 6AA, England.
- C. A. Wood, NASA Lyndon B. Johnson Space Center, Houston, TX 77058

(Received October 2, 1987;
revised February 2, 1988;
accepted February 19, 1988.)

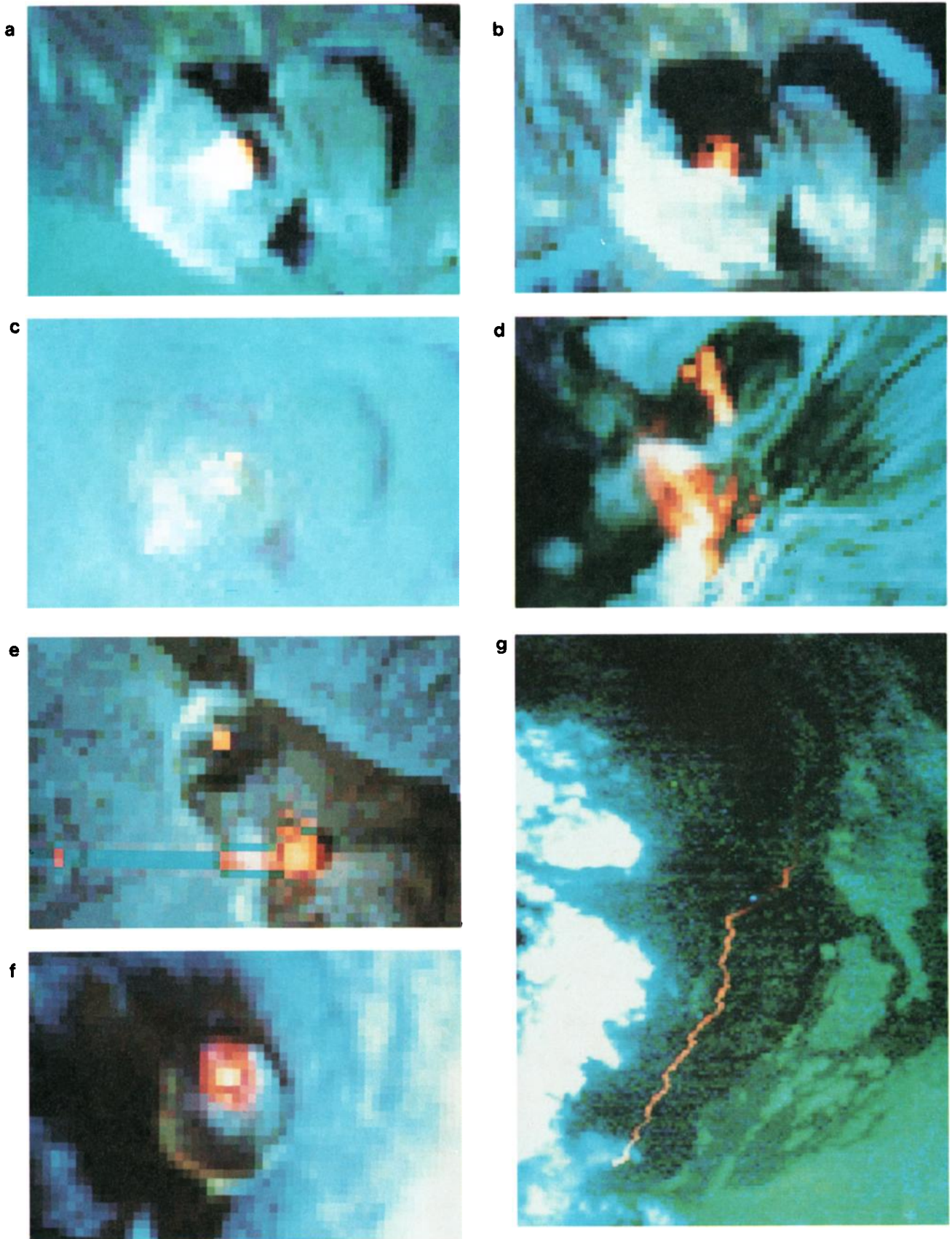


Plate 1. [*Rothery et al.* Landsat TM band 7, 5, 4 (red, green, blue) images (Plates 1a–1f). Individual pixels are 30 m by 30 m. (a) Lascar, March 16, 1985, (b) Lascar, July 21, 1985, (c) Lascar, November 12, 1986, (d) Augustine volcano, April 28, 1986, (e) Erta 'Ale, January 5, 1986, (f) Mount Erebus, January 26, 1985, (g) Landsat MSS band 7, 6, 5 (red, green, blue) image showing lava flow on Sierra Negra, November 19, 1979. Pixels represent areas of about 79 m by 58 m.